Arrhenius analysis of anisotropic surface self-diffusion on the prismatic facet of ice

Ivan Gladich[a], William Pfalzgraff[a,b], Ondřej Maršálek[a], Pavel Jungwirth[a,*], Martina Roeselová [a,*], and Steven Neshyba[b,*]

[a] Institute of Organic Chemistry and Biochemistry, Academy of Sciences of the Czech Republic and Center for Biomolecules and Complex Molecular Systems, 16610 Prague 6, Czech Republic. *Fax: +420-220 410 320; Tel:+420-220 410 313; E-mail: jungwirth@uochb.cas.cz, roeselova@uochb.cas.cz*
[b] University of Puget Sound, Tacoma, Washington, 98416, USA. *Fax: 253 879 6022; Tel: 253 879 3379; E-mail: nesh@pugetsound.edu*

Abstract:

We present an Arrhenius analysis of self-diffusion on the prismatic surface of ice calculated from molecular dynamics simulations. The six-site water model of Nada and van der Eerden was used in combination with a structure-based criterion for determining the number of liquid-like molecules in the quasi-liquid layer. Simulated temperatures range from 230 K – 287 K, the latter being just below the melting temperature of the model, 289 K. Calculated surface diffusion coefficients agree with available experimental data to within quoted precision. Our results indicate positive Arrhenius curvature, implying a change in the mechanism of self-diffusion from low to high temperature, with a concomitant increase in energy of activation from 29.1 kJ/mol at low temperature to 53.8 kJ/mol close to the melting point. In addition, we find that the surface self-diffusion is anisotropic at lower temperatures, transitioning to isotropic in the temperature range of 240-250 K. We also present a framework for self-diffusion in the quasi-liquid layer on ice that aims to explain these observations.

1. Introduction

Light-scattering properties of cirrus clouds have long been of interest because of the influence cirrus clouds exert on Earth's radiative budget, and hence climate.[1] For cloud

microphysicists, research questions typically focus on how such optical properties are related to the structure of the ice crystals that comprise those clouds. It is now well established, for example, that light scattering properties of cirrus ice crystals depend crucially on crystal habit (shape), of which a great diversity occurs in natural cirrus clouds: from simple hexagonal shapes, to hollowed forms, rosettes, and many others.[2-4] In addition, it has been hypothesized that mesoscopic (micrometer-scale) surface morphologies of ice particles can significantly influence these light-scattering properties, probably by increasing the ratio of surface area to volume.[5] Moreover, these properties are not static, but evolve continuously for a given cloud crystal. After a sufficiently long period of growth, a crystal must eventually fall and ablate in underlying warm air; its shape, mesoscopic surface properties, and radiative properties therefore undergo continuous evolution, the description of which represents considerable challenge to cloud microphysics.

Scanning electron microscopy observations of ice has revealed an unexpected way in which the above evolution takes place: the mesoscopic structure of growing and ablating ice crystals appears to occur in a distinctively facet-specific way. Prismatic facets, for example, have been found to exhibit a clear anisotropy, described as "trans-prismatic strands".[6] What might drive such anisotropy on the prismatic (but not the basal) facet?

Previous theoretical work has demonstrated that surface diffusivity can be a key factor in governing surface morphology. Mesoscopic step formation, for example, is believed to facilitate crystal growth[7, 8] as well as crystal ablation.[9] Other workers have shown that, for generic solid-vapour interfaces, different morphologies follow according to whether step growth is dynamically stable or unstable,[10, 11] and that a key factor that governs the transition between these two possibilities is the horizontal (in-plane) diffusivity of surface molecules. Importantly for our present purpose, molecular dynamics (MD) approaches have provided significant insights into these processes. MD work of Pan *et al* [12] for example, showed that

premelting begins at the corners of crystals, followed by facet-facet edges, implying that melting temperature is a function of the degree of coordination. Pereyra *et al*[13] demonstrated that stable ice nanocolumns can form spontaneously when exposed to vapour. In an MD study of the surface diffusion of ice between 180 and 210 K, Bolton and Pettersson[14] proposed a diffusion mechanism in which molecules in upper bilayers of the ice-vapour interface move horizontally by repeatedly breaking and forming hydrogen bonds. They reported an energy of activation approximately equal to that of a single hydrogen bond for molecules in the uppermost bilayer. Subsequent MD investigation by Bishop *et al* [15] of vapour-exposed basal surfaces of ice showed that the outermost, weakly-adsorbed water molecules exhibit "extraordinary diffusivity", being an order of magnitude faster than other surface molecules. Further MD work by Pfalzgraff *et al*[16] (henceforth PNR) showed that surface diffusion on vapour-exposed prismatic (and pyramidal) facets is anisotropic at a simulated temperature of 250 K. PNR hypothesized that this molecular-level anisotropy could be a mechanism by which the observed mesoscopic trans-prismatic strands occur.

There are significant barriers to readily accepting such a hypothesis, which the present paper seeks to explore. It has long been understood that anisotropic diffusivity is to be expected on crystalline facets at low temperature, before any surface premelting occurs. At high temperature, however, it is not obvious that such an expectation is well justified: a thick enough quasi-liquid layer (QLL) would be expected to hide the underlying crystalline structure, and thereby eliminate this anisotropy. As the PNR study conducted simulations only at 250 K, it is not clear what effect a warmer and thicker (or colder and thinner) QLL might have. Finally, PNR simply equated the number of liquid-like molecules involved in surface diffusion to a single surface bilayer. This approach is unsuitable for temperature-dependent studies, since in general we expect the number of liquid-like molecules at the surface of ice to increase with increasing temperature[17].

In this paper, we have employed a structure-based criterion for determining the number of liquid-like molecules in the QLL, and we use those results to explore the temperature dependence of water diffusivity at the prismatic ice/vapour interface. In the context of an Arrhenius analysis, we investigate the barrier height of in-plane diffusion, and by comparing energies of activation for the two in-plane directions we explore the anisotropy of surface diffusion.

2. Methods

2.1 Simulation Details

Molecular dynamics simulations were performed using the six site water model of Nada and van der Eerden (NE6)[18], which has an estimated melting temperature T_m = 289 K[19]. An initial crystal of hexagonal ice (I_h) at 0 K was constructed using the proton disordering algorithm of Buch *et al*[20], which specifies orientations of water molecules such that ice I_h Bernal-Fowler constraints for each molecule are satisfied[21]. The coordinate system is such that the *y* axis is normal to the (primary) prismatic facet $(10\bar{1}1)$ and coincides with the crystallographic *a* axis; the *z* axis is normal to the basal (0001) facet and coincides with the crystallographic *c* axis. Dimensions of the initial ice sample were approximately 5.4 nm x 4.7 nm x 3.7 nm in the *x*, *y*, *z* directions, respectively, for a total of N_{slab}=2880 water molecules. In the *y* direction, this configuration is comprised of 12 bi-layers of 240 molecules each.

Starting from the initial configuration, the ice sample was annealed using a constant pressure simulation (NpT) of bulk ice at zero pressure by increasing the temperature from 0 K to one of the target temperatures (230, 240, 250, 260, 270, 280, or 287 K) linearly over the course of 1.5 ns, followed by 1 ns equilibration at the target temperature. A time step of 1 fs was used for the annealing. As a final step, the *y*-dimension of the simulation box was enlarged to 12 nm, producing thus an ice slab with two prismatic facet/vacuum interfaces in

the *xz* plane. Similar protocols for slab ice equilibration have been successfully used elsewhere[17,22].

Production runs at each target temperature consisted of a constant volume (NVT) simulation of 100 ns with a time step of 2 fs. Configurations were saved at 1 ps intervals for further analysis. The first 4 ns of each trajectory were excluded from the analysis to allow for the formation of a well-equilibrated QLL. All simulations were performed using GROMACS 4.5.4[23] in double-precision floating-point arithmetic using a leap-frog integrator algorithm[24]. A cut-off of 1 nm was used for the real-space Coulomb and van der Waals interactions. Long-range Coulomb interactions were evaluated using the particle-mesh Ewald method[25,26] with a relative tolerance of 10^{-5}, fourth-order cubic interpolation and a Fourier spacing parameter of 0.12. GROMACS 4.5.4 provides a dispersion correction to the energy and the pressure for the truncated Lennard-Jones in homogeneous systems[27]; due to the inhomogeneity of our system containing the ice/vacuum interface no dispersion correction was used in this work. A canonical ensemble velocity-rescaling temperature coupling scheme[28] with a time constant of 0.1 ps was used to control the temperature. For the NpT equilibration of the systems, the Parrinello-Rahman barostat[29] was used with a time coupling constant of 2 ps.

The above simulation setup is an improvement over that employed by PNR[16] in several ways. The velocity-rescaling temperature coupling scheme[28] used here has a generalized energy that should be conserved in an NVT simulation. In the setup used by PNR, which employed the Berendsen coupling scheme for temperature control[30], total energy in an NVE test exhibited a drift of -1.4 k_BT/ns per degree of freedom. In the present setup, the drift was reduced to 4×10^{-3} k_BT/ns per degree of freedom. In addition, since the simulated system is comprised of water molecules only, the SETTLE algorithm for constraining bond lengths and angles is more efficient and accurate for our purpose than the LINCS algorithm

used in PNR. These improvements in efficiency made it possible to increase the integration time step to 2 fs, compared to 1 fs in PNR, while still improving the quality of integration. Along with faster computing resources, these changes permitted the introduction of other improvements that were not previously practical: floating-point precision was increased to double precision, whereas PNR used single precision. A cutoff of 1 nm captured interactions more realistically compared to the cutoff of 0.7 nm used by PNR. Finally, the list of molecules within the cutoff, called the "neighbour list", was updated every integration step, whereas PNR used an update interval of 5 integration steps.

2.2 Structure analysis

In order to calculate the diffusion coefficient of water on the surface of ice from MD simulation of an ice slab, it is necessary to determine the number of liquid-like water molecules at the ice/vapour interface, designated here as N_{LL}. For this purpose we used the orientational tetrahedral order parameter introduced by Errington and Debenedetti[31]. This parameter is defined as

$$q_i = \left[1 - \frac{3}{8} \sum_{j=1}^{3} \sum_{k=j+1}^{4} \left(\cos(\theta_{i,j,k}) + \frac{1}{3} \right)^2 \right] \quad (1)$$

where the sum runs over the four nearest-neighbour oxygens of the oxygen atom belonging to the i^{th} water molecule, while the angle $\theta_{i,j,k}$ is the angle formed by the oxygens *j*, *i* and *k*, with the oxygen *i* as angle vertex. In the bulk ice crystal, the four nearest-neighbour water molecules are tetrahedrally located around the central i^{th} water molecule, in a configuration that yields $q = 1$. Liquid-phase water molecules, in contrast, typically exhibit values of q smaller than 1 because the tetrahedral arrangement is distorted. The basis for discriminating between ice-like and liquid-like molecules, therefore, is to assign a threshold order parameter

q_t such that $q>q_t$ implies ice-like, and $q<q_t$ implies liquid-like character of the water molecule. This threshold is chosen using the approach of Conde *et al*[17], in which q_t is defined as the value of q such that the probability of incorrectly assigning a liquid-like molecule as ice-like is equated to the probability of incorrectly assigning an ice-like molecule as liquid-like, i.e.,

$$\int_0^{q_t} p(q;ice)\,dq = \int_{q_t}^{1} p(q;liq)\,dq \qquad (2)$$

where *p(q;ice)* and *p(q;liq)* are probability densities for bulk ice and bulk liquid water, respectively.

The threshold value q_t varies from one water model to another. In order to determine q_t for the NE6 water model, we performed two independent simulations of bulk liquid and bulk I_h ice. The two systems consisted of 894 water molecules equilibrated at the melting temperature (289 K) and pressure of 1 bar following the protocol described above. 1.5 ns production runs at 1 bar and at 298 K were then performed for the bulk systems and the last 1 ns of the production runs was used to calculate *p(q;ice)* and *p(q,liq)*. The resulting distributions are displayed in Fig. 1. Using Eq. (2) we obtained a value of q_t = 0.9264 for the NE6 water model. This value is about 2% higher than the values reported by Conde *et al*[17] for several different 3- and 4-site water models. This small difference is believed to be related to over-structuring of liquid water by the NE6 model which manifests itself, for example, in underestimation of the supercooled liquid water density[18].

The choice of the above definition of the "liquid-like" layer derives from the observation that structure within the QLL renders the distinction between ice-like and liquid-like molecules more complex than is possible to achieve merely on the basis of the

geometrical thickness of the QLL. For example, in a previous paper[32], it was demonstrated that some molecules belonging to the QLL of vapor-exposed basal ice facets (at 250 K) possess angular orientations similar to the underlying crystal, while others have angular orientations that are not found in the underlying crystal. In similar fashion, Bishop *et al*[15] reported a distinctly inhomogeneous surface structure at some temperatures, in which large "crevasses" appear. In short, because the QLL is neither homogeneously structured nor homogeneously dynamic, a scheme is required that identifies liquid-like molecules regardless of where they appear in the slab; one such scheme is provided by the above procedure. It is a compromise criterion, in that amorphous, but immobile water molecules will be counted as liquid-like, as will be the molecules in the outermost layer of ice because of the lack of enough hydrogen bonding partners. We note that Conde *et al*[17] also recognize that this approach will tend to overestimate the number of liquid-like molecules, and apply a correction based on very low-temperature ice where there should be no liquid-like molecules. We discuss the consequences of that overestimation below. We believe, however, that while this approach is based on purely structural, rather than dynamical considerations, it does acknowledge the inhomogeneity of the premelted layer and is able to provide reasonable estimates of an average number of liquid-like molecules present at the surface of ice.

2.3 Diffusivity analysis

The one-dimensional diffusion coefficients (D_i, $i = x$ or z) were obtained using Einstein's relation[33]

$$D_i = \frac{1}{2}\frac{dMSD_i(t)}{dt} \tag{3}$$

where $MSD_i(t)$ indicates the slab average of squared, one-dimensional molecular displacements as a function of time. It is noteworthy that the slab diffusion coefficient

given by Eq. (3) does not a priori exclude any molecule based on where it is in the slab. Sublimating water molecules, denoted here as N_{EV}, were excluded from the calculation of MSD because these molecules generally move considerable horizontal distances while in transit from one slab surface to another; including them in the MSD plot would tend to bias high the resulting diffusion coefficient. The GROMACS utility g_msd[27] was used to obtain the MSD plot. Thus, multiple $MSD_i(t)$ functions from a given trajectory, differing from one another in starting time (advanced in intervals of 20 ps), were averaged, and the resulting $MSD_i(t)$ plot was fit to a straight line using a least-squares algorithm. The diffusion coefficient, D_i, was then obtained from the slope of the linear fit using the most statistically relevant part of the $MSD_i(t)$ plot, which we determined as the time window between 5 and 25 ns.

Since the molecules in bulk ice are immobile on the time scale of our simulation and do not contribute to the MSD, they need to be excluded when determining a diffusion coefficient from the slope of the MSD plot obtained for the entire ice slab. This is likely to be true also for the ice-like molecules located in the interfacial layer. We therefore assume that it is only the liquid-like molecules that contribute to surface diffusivity. The one-dimensional surface diffusion coefficients, D_i^*, are thus calculated according to[16]

$$D_i^* = D_i / Q \tag{4}$$

where Q is the ratio of the average number of liquid-like molecules (N_{LL}) to the total number of molecules of the system (N_{Slab}). Because all molecules that sublimated from one or the other surface of the ice slab during the simulation (N_{EV}) were *a priori* excluded from the MSD analysis, values of Q were obtained using

$$Q = (N_{LL} - N_{Ev}) / (N_{Slab} - N_{Ev}) \quad (5)$$

As regards the evaluation of the scaling parameter, Q, Eq. 5 represents a refinement of the approach employed in the previous study by PNR[16] where the number of liquid-like molecules at 250 K was simply equated to the number of molecules constituting one ice bilayer and the (relatively few) sublimating molecules were not taken into account in the calculation of Q (cf. Eq. 6 of PNR[16]). Finally, we note that the two-dimensional in-plane surface diffusion coefficient can be constructed by

$$D_{xz}^{*} = \left(D_{x}^{*} + D_{z}^{*}\right) / 2 \quad (6)$$

3. Results

The effect of temperature on the surface structure and diffusivity of the prismatic ice facet was studied through a series of simulations of an ice slab with the prismatic face as the free surface at temperatures between 230 K and 287 K. These simulation temperatures correspond to undercooling of –59 through –2 degrees relative to the melting point of the NE6 water model (T_m = 289 K). The ice slabs were found to retain well-defined crystalline structure in their interiors, at all simulated temperatures. Surface reconstruction at both ice/vapour interfaces consisted of development of a disordered, quasi-liquid interfacial layer (QLL) within a few nanoseconds from the simulation start. As we will argue below, much of the temperature dependence of diffusivity can be attributed to changes in the thickness and liquid-like nature of molecules in the QLL.

On the basis of instantaneous structural disorder alone, the snapshots shown in Figure 2 indicate that the thickness of the surface region increases with increasing temperature. The density profiles shown in Figure 3 provide additional, layer-specific information about this

disorder. In the direction normal to the prismatic plane (the *y* axis), the ice crystal lattice consists of bilayers giving rise to double peaks in the density profiles. Each peak of the bilayer dublet corresponds to three oxygen atoms of an hexagonal ring, the first three oxygens having a somewhat different *y* coordinate than the other three. At the lowest temperature (230 K), only the outermost bilayer (denoted ε_2) is involved in the formation of liquid-like surface layer, and surface relaxation due to deviations of the interfacial water molecules from the ideal crystalline lattice positions is reflected in the reduced peak heights and broadening of the bilayer doublet. At the same time, a small fraction of water molecules leaves the ε_2 bilayer, leaving vacancies in it, to form an incomplete external layer (denoted as ε_1).

Upon increasing the temperature, the widths of the density profile peaks increase while the peak heights decrease, both as a result of increasing amplitudes of thermal motion of molecules in the ice lattice. The broadening of the peaks and reduction of the peak heights is most pronounced in the surface layers. Qualitatively, the T=287K panel of Figure 3 (two degrees below the NE6 bulk melting temperature) suggests that the QLL involves the two outermost ice bilayers, i.e., $\varepsilon_1 + \varepsilon_2$ merged with μ_1. The temperature dependence of the density profiles of the prismatic ice surface described above is quite similar to that reported by Bishop *et al*[15] for the basal ice surface using the same water model (NE6). It is also similar to results reported by Conde *et al*[17] for several other water models. Quantitative investigation of the QLL thickness at temperatures approaching more closely the melting point using MD simulations is at present hampered by limited system sizes that one can typically afford to simulate, and by relatively large uncertainties (~3 K) in the melting temperatures of water models determined from MD simulations[17].

Because density profiles depict average positions, they do not provide enough information to distinguish ice-like from liquid-like molecules. For this purpose, we employ

the structure analysis described in Section 2.2 to calculate the instantaneous number of liquid-like molecules, N_{LL}. Figure 4 shows N_{LL} as a function of simulation time for selected temperatures in the range between 230 K and 287 K. Averaged N_{LL} values are given in Table 1. As can be seen, the number of liquid-like molecules increases with increasing temperature. At the same time, the fluctuations around the corresponding average values also increase. This behavior is qualitatively consistent with that reported for other water models[17], although the fluctuations obtained here appear to be larger as the temperature approaches the melting point: for the TIP4P/Ice model, the maximum fluctuations of the instantaneous number of liquid-like molecules are about ±10 per cent close to its melting temperature of 271 K[17], whereas in the present study the fluctuations reach almost ±20 per cent at 2 degrees below the melting point. We attribute this difference to the significantly higher absolute value of the melting point of the NE6 model compared to the other water force fields.

Although not required for the calculation of diffusion coefficients, the thickness of the QLL is nevertheless of interest in the present context because of the influence the underlying ice-like "terrain" may exert on horizontal diffusion of liquid-like molecules. QLL thickness (denoted δ) can be estimated by equating the number of liquid-like molecules evaluated from the simulation of the free ice surface to that of a box of liquid water of dimensions *Lx Lz* δ using[17]

$$\delta = \frac{N_{LL} M}{2 \rho N_A L_x L_z} \tag{7}$$

where N_{LL} is the number of liquid-like molecules introduced in Section 2.2, M is the molar mass of water, ρ is the density of liquid water, N_A is Avogadro's number, and $L_x L_z$ is the area of the interface. The factor of 2 in the denominator accounts for the fact that the ice slab has two interfaces. Results are summarized in Table 1. We note that the lateral dimensions of the

ice block, L_x and L_z, change slightly with temperature. To compute the QLL thickness, however, we neglect these small changes and use the values given in Section 2.1. Concerning the density of water, ρ, we use the temperature dependent values reported by Nada and van der Eerden for the supercooled liquid water modelled by the NE6 potential[18]. (Using a constant value of 0.99 g/cm^3 for the density of NE6 water close to the melting point[18] over the entire temperature range considered here yielded results for δ that are almost identical at the higher temperatures, and smaller by about 10 per cent at the low temperatures.) Fluctuations in the instantaneous number of liquid-like molecules are reflected in fluctuations in the QLL thickness of about ±0.15 nm at the highest temperature close to the melting point, whereas at the lower temperatures the fluctuations are substantially smaller.

We note that the values of δ obtained using Eq. 7 and presented in Table 1 should be considered as upper bounds of the average QLL thickness. This is because the calculation of N_{LL} overestimates the number of liquid-like molecules in the QLL due to having all water molecules in the outermost layer of ice classified as liquid-like merely because these molecules, being located at the ice/vapour interface, are not able to form four hydrogen bonds. This results in rather low values of the tetrahedral order parameter *q* of the surface molecules, which thus automatically fall into the "liquid" category, regardless of their true ice- or liquid-like character. In addition, a low value of *q* can also be obtained for an amorphous solid water structure, in which the water molecules are mainly four-coordinated, but are in a distorted tetrahedron arrangement. Such water molecules will be incorrectly classified as liquid-like, though they do not constitute a quasi-liquid as their mobility is very low. For these reasons, Eq. 7 is likely to overestimate the QLL thickness, in particular at low temperatures. While at high temperatures the majority of both non-tetrahedral as well as non-four-coordinated (surface) water molecules can be classified as liquid-like because they have high mobility, the discrepancy between the calculated N_{LL} and the true number of liquid-like

molecules increases with decreasing temperature. As noted by Conde *et al*[17], at low temperatures the difference between the "true" thickness of the QLL and the "apparent" one (as predicted by Eq. 7) can be 0.25 – 0.3 nm[17], i.e., as much as one water layer.

Finally, comparison of QLL thickness obtained in the present study with results reported for the prismatic face by Conde *et al*[17] reveals that the NE6 model systematically predicts somewhat lower QLL thickness than the TIP4P/Ice model when compared at the same undercooling with respect to the melting point of each model. This can be rationalized, at least partially, by the somewhat larger value of the q_t parameter reflecting the over-structuring of liquid water by the NE6 model. Thus, the NE6 model is likely to yield a smaller number of liquid-like molecules (i.e., thinner QLL) than some of the most popular 3- and 4-site models at the same degree of undercooling relative to the melting temperature.

Also shown in Table 1 is the total number of molecules that sublimated from one or the other surface of the ice slab during the simulation, N_{EV}, which is needed to evaluate the diffusion scaling factor Q using Eq. 5. In addition, we present the quantity N_{LL} - N_{EV} to demonstrate that despite the increasing number of sublimating molecules (which are excluded from the MSD analysis) with increasing temperature, enough liquid-like molecules remain to provide statistical confidence in the calculated values of Q.

We now turn to an investigation of in-plane diffusion. Figure 5 shows a 30 ns segment of a trajectory for a representative surface molecule at the coldest modeled temperature, 230 K. The top panel shows the vertical (y-coordinate) position of the molecule. Most of the time, the molecule is located in the ε_2 sub-layer, with a single excursion to the ε_1 sublayer lasting ~5 ns (marked in the figure by the two vertical lines). The lower two panels show that both vertical transitions (to ε_1 and back to ε_2) occur in concert with much larger out-of-plane displacements (note the difference in vertical scales), therefore these transitions will contribute to surface diffusion coefficients D_x^* and D_z^*. Importantly to our present purpose,

these contributions are potentially different in *x* vs. *z* direction and, thus, could lead to diffusive anisotropy. Focusing next on the 5 ns interval during which the molecule was in the ε_1 sub-layer, we note three qualitatively distinct in-plane transitions. Label A marks abrupt movement of the molecule ~1 nm in x-direction, while it remains at the same z-location. Label B marks a converse motion: the molecule moves abruptly ~1 nm in z-direction, while remaining at the same x-location. The molecule remains in the ε_1 sub-layer during both events. A third label, C, appears to represent concerted in-plane motion in which the molecule is displaced in both in-plane directions simultaneously. Since all three transitions are potentially characterized by distinct energies of activation, they too could lead to diffusive anisotropy. For the time during which the molecule is in the ε_2 sub-layer, the molecule is largely immobile in-plane. The sole significant in-plane excursion, marked as B^*, occurs at t ~ 29.5 ns, at which time the molecule moves abruptly in the z direction; the motion of the ε_2 molecule marked as B^* is thus analogous to B of ε_1. Movements of ε_2 molecules analogous to A and C of ε_1 were also observed (not shown). Therefore, in-plane transitions of molecules in the ε_2 sub-layer could also lead to diffusive anisotropy, in a similar way as in the case of ε_1 molecules.

Summarizing the low-temperature results, we conclude that the diffusion mechanism suggested by Bishop *et al*[15] and by Bolton and Pettersson[14], in which the outermost molecules (ε_1 and, to some degree, also ε_2) move atop a relatively rigid terrain is supported by the present results. Hereinafter we will refer to this mechanism as "facet-proximate", to distinguish it from mechanisms that appear at higher temperatures (*vide infra*). In general, facet-proximate diffusion is strongly influenced by the geometry of the underlying crystalline terrain; it will depend on distinct transition states in the two in-plane directions, and therefore will potentially give rise to diffusive anisotropy whenever the underlying crystalline geometry is anisotropic. Figure 6 displays schematically the types of facet-proximate

diffusion movements observed here. Which mechanisms can be expected to dominate the diffusion at this temperature? Although a quantitative answer is beyond the scope of the present paper, it is likely that the least contribution (based on these trajectory results) will come from diffusion within ε_2, since in-plane displacements associated with such transitions are generally much smaller, and less frequent, than in-plane displacements associated with ε_1. (As an example, compare the *x* and *z* displacements at marker B^* to the displacements at A-C in Fig. 5.)

We turn next to an investigation of in-plane diffusion at a high temperature, close to the melting point. Fig. 7 shows the results for 287 K. As can be seen in the top panel, at this temperature, there is frequent vertical exchange not only between sublayers ε_1 and ε_2, but the vertical mobility is extended to the underlying μ_1 and, to a certain degree, also μ_2 bilayers, which were both fully crystalline at the low temperature. Two qualitatively distinctive states are apparent. Marker D points to relatively immobile states in which the molecule is stuck in the outer or inner parts of the μ_1 bilayer. Diffusion in these states is analogous to that of the facet-proximate mechanisms at low temperature, however, only very little in-plane displacement appears on this scale . Much larger in-plane motion is associated with a second state, marked as E. Diffusion corresponding to marker E appears to coincide with rapid cycling between sublayers ε_1 and ε_2 (the distinction between which is thereby largely lost) in concert with extensive in-plane displacements. The diffusion may therefore be described as quasi-3-dimensional, with much smaller excursions in the vertical (y-direction) than in the in-plane directions. Hereinafter we will refer to this mechanism as "facet-distant", since at this temperature the outer part of the QLL lies relatively far from the underlying crystalline terrain. Importantly for our present purpose, facet-distant diffusion may be expected to have a higher energy of activation than facet-proximate diffusion, because the vertical motion takes a molecule from a more hydrated environment close to the surface where fewer hydrogen

bonding partners are available. It is also expected to be isotropic in the in-plane direction because of the greater thickness of the QLL at higher temperature.

The foregoing analysis depends on inspection of individual molecular trajectories, of which we presented representative examples at the two extreme temperatures simulated. In an effort to understand the transition between the facet-proximate and facet-distant regimes, we next turn to statistical measures of in-plane motion. Figure 8 shows 1-dimensional mean-squared displacement functions for slabs of selected temperatures, prepared as described in Section 2. The slab diffusion coefficients, D_x and D_z, are proportional to the slopes of these curves, from which we obtain surface diffusion coefficients, D_x* and D_z* using Eqs. 4 and 5. Table 2 and an Arrhenius plot (Fig. 9) summarize the results. The data suggest that significant anisotropy occurs only at lower temperatures, a matter discussed in more detail below. The negative slope in the Arrhenius plot indicates a positive activation energy, E_a, throughout the temperature range. In addition, the function is characterized by a distinct positive curvature, which has been fit by a quadratic least-squares algorithm (solid line in Fig. 9). Conventional Arrhenius analysis of these properties is to infer a change in diffusion mechanism over the observed temperature range. Because the curvature of ln D^* vs 1/T is positive, we further infer that E_a of the high-temperature mechanism is greater than E_a of the low-temperature mechanism. This interpretation is subject to the usual assumptions of Arrhenius analysis, e.g., that the Arrenius prefactor is temperature independent. Values of $E_a(T)$ calculated from the quadratic best-fit parameters from the Arrhenius plot are shown in Fig. 10. The low-temperature value of E_a = 29.1 kJ/mol corresponds approximately to one hydrogen bond (the average hydrogen bond strength obtained with the NE6 model for bulk ice I_h is 24.5 kJ/mol)[14, 16], increasing to about two hydrogen bonds (E_a = 53.8 kJ/mol) close to the melting point.

For comparison, we also present in Figure 9 results from other studies of self-diffusion in liquid water on the surface of ice. Nasello *et al* carried out measurements of the surface diffusivity of ice by tracking the formation of grain boundary grooves on surfaces of polycrystalline ice[34]. The present results appear to be consistent with their measurements because they lie within quoted experimental error bars. This consistency would remain valid even if we corrected the MD temperatures to under-melting temperatures, which would shift the black MD curve slightly to the right in Figure 9. However, the large uncertainty of the experimental values does not allow to test the validity of the curvature of the Arrhenius plot or the anisotropy we have obtained here. It is also important to note that assumptions built into the calculation of surface diffusivity by Nasello *et al* are not possible to reproduce in the present context. In particular, Nasello *et al* invoke the assumption that grain boundary groove formation occurs only by surface diffusion. Our expectations for quantitative agreement with their results are therefore constrained in ways that we have not evaluated quantitatively.

Also shown are experimental results of Price *et al*[35] for supercooled liquid water, and MD results of Carignano *et al*[36] for NE6 bulk liquid water, indicating that the NE6 water model has somewhat slower dynamical properties than those observed experimentally for supercooled water. Although surface diffusivity is not, in general, expected to be identical to bulk diffusivity, it has been noted that surface diffusion coefficients for ice *are* close to those of bulk liquid water[37,38]. It is gratifying to note that agreement is within an order of magnitude over the temperature range considered. Perhaps the more important comparison is qualitative: the bulk liquid measurements in the supercooled water exhibit distinct negative Arrhenius curvature, meaning activation energy of diffusion decreases with increasing temperature, the opposite of what we observe for surface diffusion on ice. In addition, the results for supercooled bulk water imply that E_a is equivalent to about one hydrogen bond at freezing temperature and about two hydrogen bonds at 230 K[35], whereas the present work

implies that E_a is equivalent to about two hydrogen bonds at freezing and one hydrogen bond at 230 K. These observations indicate radically different mechanisms for diffusion in supercooled liquid water *vis a vis* surface diffusion of ice.

Figure 11 displays the ratio of diffusion coefficients in the two in-plane directions, $\frac{D_x^*}{D_z^*}$, which we take to be a quantitative measure of the diffusive anisotropy. The figure suggests that a qualitative change occurs between 240 K and 250 K, with distinct anisotropy appearing only in the lower temperature range. It is interesting to note that Bishop *et al*[15] also remarked on a qualitative change in surface topography at 240-250 K, albeit of the basal surface. They ascribed this change to the appearance of three-coordinated molecules in the ε_2 sub-layer as temperature increases.

In our view, the facet-distant/facet-proximate framework discussed earlier has the potential to explain nearly all the above described observations. At low temperatures, the framework stipulates that facet-proximate diffusion mechanisms dominate. The observed anisotropic diffusivity at 230-240 K is consistent with this picture, since the underlying crystalline terrain is the highly anisotropic prismatic facet. It is noteworthy that the low-temperature activation energy of ~1 hydrogen bond obtained here is also consistent with the low-temperature MD study of Bolton and Pettersson[14]. At high temperatures, on the other hand, the framework stipulates that facet-distant mechanisms dominate, and that surface diffusion should become isotropic. The observed transition to isotropic diffusivity around T ~ 250 K is also consistent with this picture, as is the tendency to higher energy of activation with increasing temperature.

Finally, it is useful to consider the consequences of overestimating N_{LL} as a result of including amorphous ice molecules in the accounting of liquid-like molecules, as alluded to in Section 2.2. We note first that the diffusive surface anisotropy, $\frac{D_x^*}{D_z^*}$, is insensitive to the

definition of N_{LL}, because the factor Q cancels when taking the ratio (see Eqs. (4-5)). Second, the positive Arrhenius curvature shown in Figure 9 would be even more exaggerated if we have underestimated the diffusivity by overestimating Q at low temperatures.

4. Conclusions

We have presented an Arrhenius analysis of MD-simulated self-diffusion on the surface of an NE6 ice slab in which the prismatic facet is exposed to the vapour phase. Simulated temperatures range from 230 K to 287 K, the latter approaching the melting temperature of NE6 ice (T_m = 289 K). Calculated surface diffusion coefficients agree with available experimental data to within quoted precision for the entire temperature range. Our results indicate positive Arrhenius curvature, implying a change in the mechanism of self-diffusion from low to high temperature, with a concomitant increase in energy of activation. Since supercooled water is known to exhibit the opposite trend (energy of activation is a decreasing function of temperature), we infer that self-diffusion at ice surface occurs by significantly different mechanisms compared to bulk self-diffusion in supercooled water. In addition, we find that self-diffusion on the prismatic ice surface is anisotropic at lower temperatures, transitioning to isotropic in the temperature range of 240-250 K.

We have also presented a framework for self-diffusion on the surface of ice that aims to explain these observations. According to this framework, diffusion of liquid-like molecules within the quasi-liquid layer (QLL) on ice is understood to take place on a fixed underlying crystalline terrain. Mechanisms of in-plane diffusion vary according to the thickness of the QLL (which is temperature-dependent) and on the directional anisotropy of the underlying crystalline terrain (which is facet-dependent). At low temperature, a thin QLL implies that most liquid-like molecules are “facet-proximate”, i.e., strongly influenced by the geometry of the underlying crystalline terrain. When the exposed facet is directionally anisotropic, facet-

proximate diffusion will depend (in general) on distinct transition states in the two in-plane directions, and therefore can be expected to lead to anisotropic diffusion. At high temperature, in contrast, a thick enough QLL admits the possibility that most liquid-like molecules are "facet-distant", i.e., negligibly influenced by the underlying crystalline terrain. In-plane diffusion of these molecules is instead governed by quasi-3-dimensional liquid-like mechanisms that are isotropic regardless of the geometry of the underlying crystalline terrain. The observed transition from anisotropic to isotropic self-diffusion (with increasing temperature) occurs as a result of a transition from facet-proximate to facet-distant diffusion as dominant mechanisms. The framework is also consistent with previous work in our group (PNR[16]) in which anisotropic diffusion was found at 250 K for directionally anisotropic prismatic and pyramidal facets, but not for the basal facet, which possesses only slight directional anisotropy.

Given that anisotropy of surface diffusion is a widely accepted concept in solid state surface science, it is perhaps surprising that it has not been established experimentally for ice. Our results indicate that experimentalists should look at temperatures below 250 K for possible evidence of the diffusive anisotropy on ice, on strongly directionally anisotropic facets such as the prismatic or pyramidal. Our future theoretical work will focus on identifying transition states for the facet-proximate diffusion mechanism, and on how these molecular level processes relate to the experimentally observed mesoscopic structure of cirrus ice analogues.

Acknowledgements

This research was supported by the Czech Science Foundation (grant P208/10/1724), the Ministry of Education of the Czech Republic (grants ME09064 and LC512), the U.S. National Science Foundation (grant CHE-0909227), and by the University of Puget Sound.

P.J. wishes to acknowledge the support from the Academy of Sciences (Premium Academiae). S.N. thanks Penny Rowe for fruitful discussions.

References

1. G. L. Stephens, S. C. Tsay, P. W. Stackhouse and P. J. Flatau, *Journal of the Atmospheric Sciences*, 1990, **47**, 1742-1753.
2. Y. Takano and K. N. Liou, *Journal of the Atmospheric Sciences*, 1995, **52**, 818-837.
3. S. Kinne and K. N. Liou, *Atmos. Res.*, 1989, **24**, 273-284.
4. S. C. Ou, K. N. Liou, Y. Takano, N. X. Rao, Q. Fu, A. J. Heymsfield, L. M. Miloshevich, B. Baum and S. A. Kinne, *Journal of the Atmospheric Sciences*, 1995, **52**, 4143-4158.
5. A. Kokhanovsky, ed. Praxis, Garrett, T., Chichester U.K., 2008, vol. 3, ch. 3.
6. W. C. Pfalzgraff, R. M. Hulscher and S. P. Neshyba, *Atmospheric Chemistry and Physics*, 2010, **10**, 2927-2935.
7. P. V. Hobbs and W. D. Scott, *Philosophical Magazine*, 1965, **11**, 1083-1086.
8. P. V. Hobbs and W. D. Scott, *Journal of Geophysical Research*, 1965, **70**, 5025-5034.
9. J. Nelson, *J. Atmos. Sci.*, 1998, **55**, 910-919.
10. G. S. Bales, R. Bruinsma, E. A. Eklund, R. P. U. Karunasiri, J. Rudnick and A. Zangwill, *Science*, 1990, **249**, 264-268.
11. G. S. Bales and A. Zangwill, *Physical Review B*, 1990, **41**, 5500-5508.
12. D. Pan, L-M Liu, B. Slater, A. Michaelides, and E. Wang, *ACS-Nano*, 2011, **5**, 4562-4569.
13. R. G. Pereyra and M. A. Carignano, *J. Phys. Chem. C*, 2009, **113**, 12699-12705.
14. K. Bolton and J. B. C. Pettersson, *Journal of Physical Chemistry B*, 2000, **104**, 1590-1595.
15. C. L. Bishop, D. Pan, L. M. Liu, G. A. Tribello, A. Michaelides, E. G. Wang and B. Slater, *Faraday Discussions*, 2009, **141**, 277-292.
16. W. C. Pfalzgraff, S. P. Neshyba and M. Roeselova, *Journal of Physical Chemistry A*, 2011, **115**, 6184-6193.
17. M. M. Conde, C. Vega and A. Patrykiejew, *Journal of Chemical Physics*, 2008, **129**, 014702-014713.
18. H. Nada and J. van der Eerden, *Journal of Chemical Physics*, 2003, **118**, 7401-7413.
19. J. L. F. Abascal, R. G. Fernandez, C. Vega and M. A. Carignano, *Journal of Chemical Physics*, 2006, **125**, 166101-1 - 166101-2.
20. V. Buch, P. Sandler and J. Sadlej, *Journal of Physical Chemistry B*, 1998, **102**, 8641-8653.
21. J. D. Bernal and R. H. Fowler, *Journal of Chemical Physics*, 1933, **1**, 515-548.
22. E. Muchova, I. Gladich, S. Picaud, P. N. Hoang and M. Roeselova, *Journal of Physical Chemistry A*, 2011, **115**, 5973-5982.
23. B. Hess, C. Kutzner, D. van der Spoel and E. Lindahl, *Journal of Chemical Theory and Computation*, 2008, **4**, 435-447.
24. R. W. Hockney, S. P. Goel and J. W. Eastwood, *Journal of Computational Physics*, 1974, **14**, 148-158.

25. T. Darden, D. York and L. Pedersen, *Journal of Chemical Physics*, 1993, **98**, 10089-10092.
26. U. Essmann, L. Perera, M. L. Berkowitz, T. Darden, H. Lee and L. G. Pedersen, *Journal of Chemical Physics*, 1995, **103**, 8577-8593.
27. D. van der Spoel, E. Lindahl, B. Hess, A. R. van Buuren, E. Apol, P. J. Meulenhoff, D. P. Tieleman, A. L. T. M. Sijbers, K. A. Feenstra, R. van Drunen and H. J. C. Berendsen, Gromas User Manual Version 4.5.4, www.gromacs.org (2010)
28. G. Bussi, D. Donadio and M. Parrinello, *Journal of Chemical Physics*, 2007, **126**, 014101-1 - 014101-7.
29. M. Parrinello and A. Rahman, *Journal of Applied Physics*, 1981, **52**, 7182-7190.
30. H. J. C. Berendsen, J. P. M. Postma, W. F. Vangunsteren, A. Dinola and J. R. Haak, *Journal of Chemical Physics*, 1984, **81**, 3684-3690.
31. J. R. Errington and P. G. Debenedetti, *Nature*, 2001, **409**, 318-321.
32. S. P. Neshyba, E. Nugent, M. Roeselová, and P. Jungwirth, *Journal of Physical Chemistry C*, 2009, **113**, 4597-4604.
33. M. Allen and D. J. Tildesley, *Computer Simulation of Liquids*, Oxford University Press Inc., Oxford, 1987.
34. O. B. Nasello, S. N. de Juarez and C. L. Di Prinzio, *Scripta Materialia*, 2007, **56**, 1071-1073.
35. W. S. Price, H. Ide and Y. Arata, *Journal of Physical Chemistry A*, 1999, **103**, 448-450.
36. M. A. Carignano, P. B. Shepson and I. Szleifer, *Molecular Physics*, 2005, **103**, 2957-2967.
37. S. Picaud, *Journal of Chemical Physics*, 2006, **125**, 174712-1 - 174712-10.
38. M. W. Mahoney and W. L. Jorgensen, *Journal of Chemical Physics*, 2001, **114**, 363-366.

Table 1: Average number of liquid-like molecules (N_{LL}) and estimated thickness of the QLL (δ) as a function of temperature, calculated using the temperature dependence of the NE6 supercooled liquid water density (ρ)[36]. T-T_m denotes the undercooling relative to the melting point of the NE6 model (T_m = 289 K). Also shown are the total number of molecules evaporated in the course of 100 ns simulation time (N_{EV}), estimated average number of non-evapourated liquid-like molecules that remain at the ice surface (N_{LL} - N_{EV}) and the scaling parameter Q defined by Eq. 5.

T (K)	T-T_m (K)	N_{LL}	ρ (g cm^{-3})	δ (nm)	N_{EV}	N_{LL} - N_{EV}	Q
287	-2	992	1.000	0.74	558	434	0.187
280	-9	740	0.995	0.55	331	409	0.161
270	-19	592	0.989	0.45	156	436	0.160
260	-29	496	0.962	0.38	47	449	0.159
250	-39	441	0.955	0.34	25	416	0.146
240	-49	402	0.925	0.32	8	394	0.137
230	-59	382	0.900	0.32	4	378	0.131

Table 2: One-dimensional surface diffusion coefficients (D^*_x and D^*_z) along the *x* and *z* directions, two-dimensional surface diffusion coefficient (D^*_{xz}) and anisotropy coefficient (D^*_x / D^*_z) as a function of temperature. T-T_m denotes the undercooling relative to the melting point of the NE6 model (T_m = 289 K). Uncertainties given in the table correspond to 99% confidence intervals and were obtained by standard error propagation, assuming that the uncertainty in the slab diffusion coefficients (D_i) reported by GROMACS corresponds to one standard deviation.

T (K)	T-T_m (K)	D^*_x (10^{-9} m^{2}s^{-1})	D^*_z (10^{-9} m^{2}s^{-1})	D^*_{xz} (10^{-9} m^{2}s^{-1})	D^*_x/D^*_z
287	-2	1.31±0.08	1.41±0.09	1.4±0.06	0.93±0.08
280	-9	0.83±0.03	0.76±0.06	0.79±0.03	1.09±0.09
270	-19	0.35±0.03	0.33±0.03	0.34±0.02	1.09±0.09
260	-29	0.162±0.003	0.1552±0.0008	0.158±0.002	1.04±0.02
250	-39	0.076±0.004	0.0741±0.0009	0.075±0.002	1.03±0.05
240	-49	0.0445±0.0008	0.0328±0.0008	0.039±0.0006	1.36±0.04
230	-59	0.0198±0.0008	0.0152±0.0008	0.018±0.0006	1.30±0.09

Figure Captions

Figure 1. Probability density distribution $p(q)$ of the orientational order parameter q of the NE6 water model obtained from simulation of bulk water (blue) and bulk ice I_h (red) at the melting point temperature of the model, 289 K, and a pressure of 1 bar.

Figure 2. Snapshots of the prismatic ice/vapour interface for selected simulation temperatures viewed along the *z* (basal) axis. The axis normal to the interface is the *y* axis.

Figure 3. Density profiles of water oxygen atoms along the surface normal (*y* axis) for selected simulation temperatures. The right-hand side of each plot corresponds to the ice/vapour interface, the left-hand side ($y = 0$) to the center of the ice slab.

Figure 4. Instantaneous number of liquid-like molecules, N_{LL}, as a function of simulation time for selected temperatures.

Figure 5. Out-of-plane (*y* coordinate) and in-plane (*x* and *z*) motion of a surface water molecule at 230 K. Dashed horizontal lines in the upper panel demark boundaries between adjacent layers. Full vertical lines bracket the time interval during which the water molecule was located in the ε_1 sub-layer. Events marked A, B, B^*, and C are discussed in the text (see also Fig. 6).

Figure 6. Schematic depiction of distinctive diffusion events identified in Fig. 5: A – jump of a molecule in the *x*-direction exclusively, B – jump of a molecule in the *z*-direction exclusively, C – jump of a molecule in *x*- and *z*-directions simultaneously.

Figure 7. Out-of-plane (*y* coordinate) and in-plane (*x* and *z* coordinates) motion of a surface water molecule at 287 K. Dashed horizontal lines in the upper panel demark boundaries between adjacent layers. Events marked D and E are discussed in the text.

Figure 8. One-dimensional in-plane mean square displacement of water oxygen atoms as a function of time for selected simulation temperatures.

Figure 9. Arrhenius plot of calculated water self diffusion coefficients D_x^* and D_z^*. Shown for comparison are the diffusion coefficient for NE6 bulk liquid water calculated by Carignano *et al*[36], experimental values of the diffusion coefficient for liquid water from Price *et al*[35], and the measured in-plane diffusion coefficient on ice surface from Nasello *et al*[34].

Figure 10. Temperature dependence of the energy of activation, E_a, of in-plane diffusion at the prismatic ice surface. The values of E_a were obtained as derivatives of the quadratic fit to the two-dimensional surface diffusion coefficient, D_{xz}^*.

Figure 11. Diffusion anisotropy coefficient (D^*_x / D^*_z) as a function of temperature.

Figure 1.

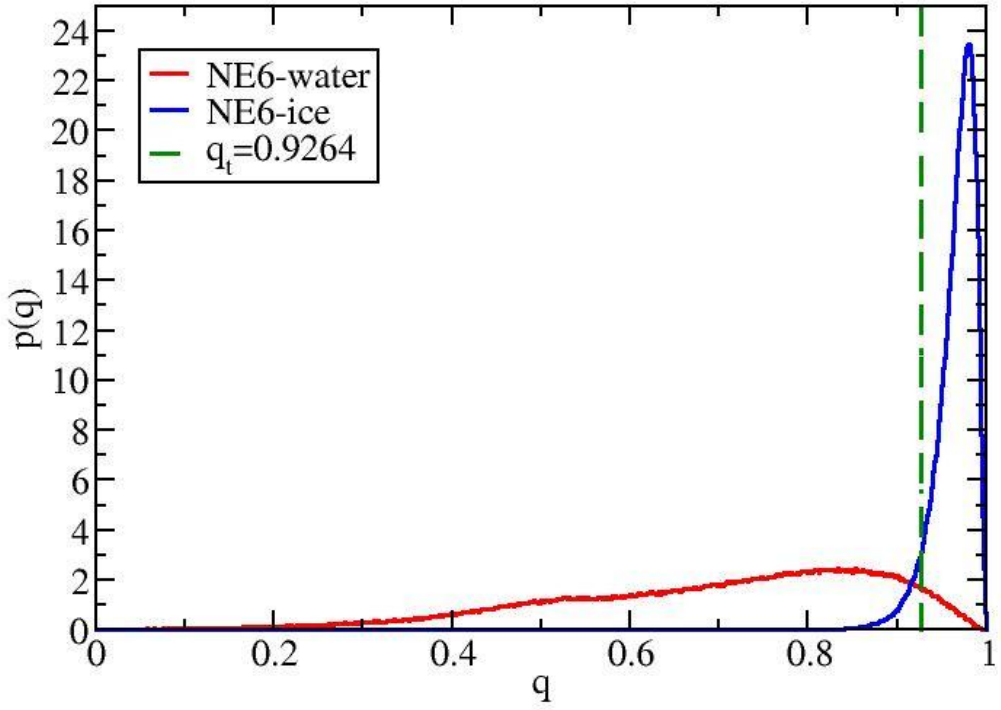
NE6-water
NE6-ice
q_t=0.9264
p(q)
q
0
2
4
6
8
10
12
14
16
18
20
22
24
0
0.2
0.4
0.6
0.8
1

Figure 2.

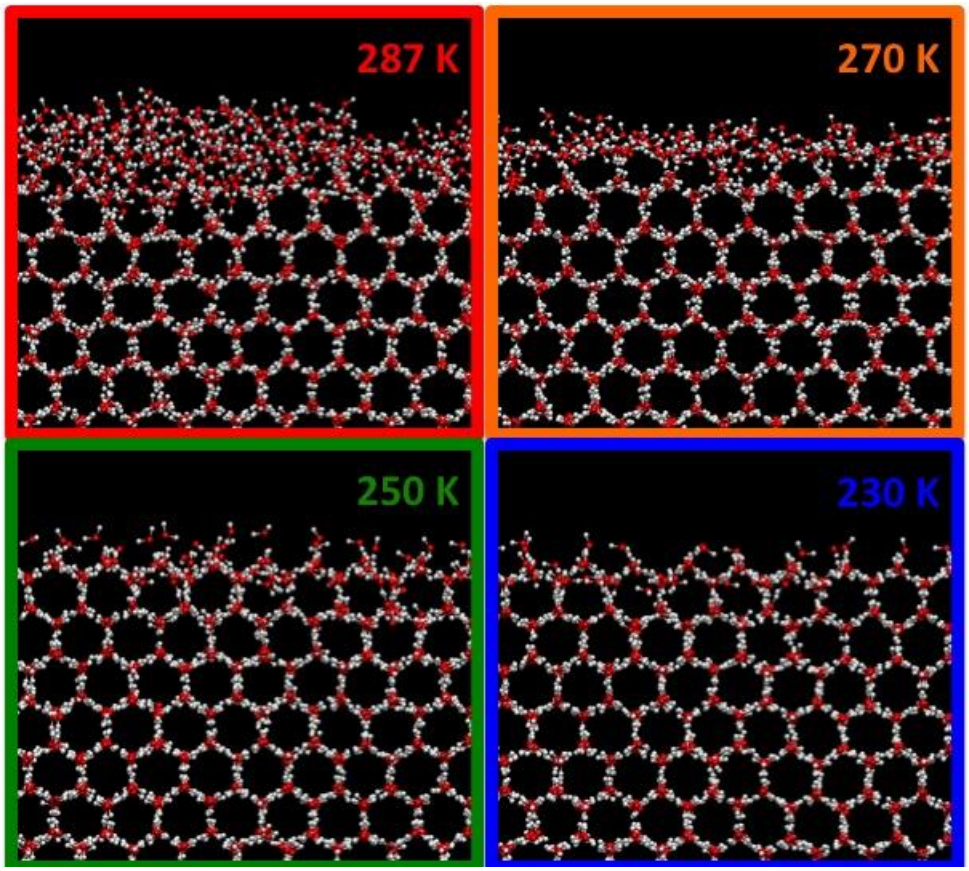

Figure 3.

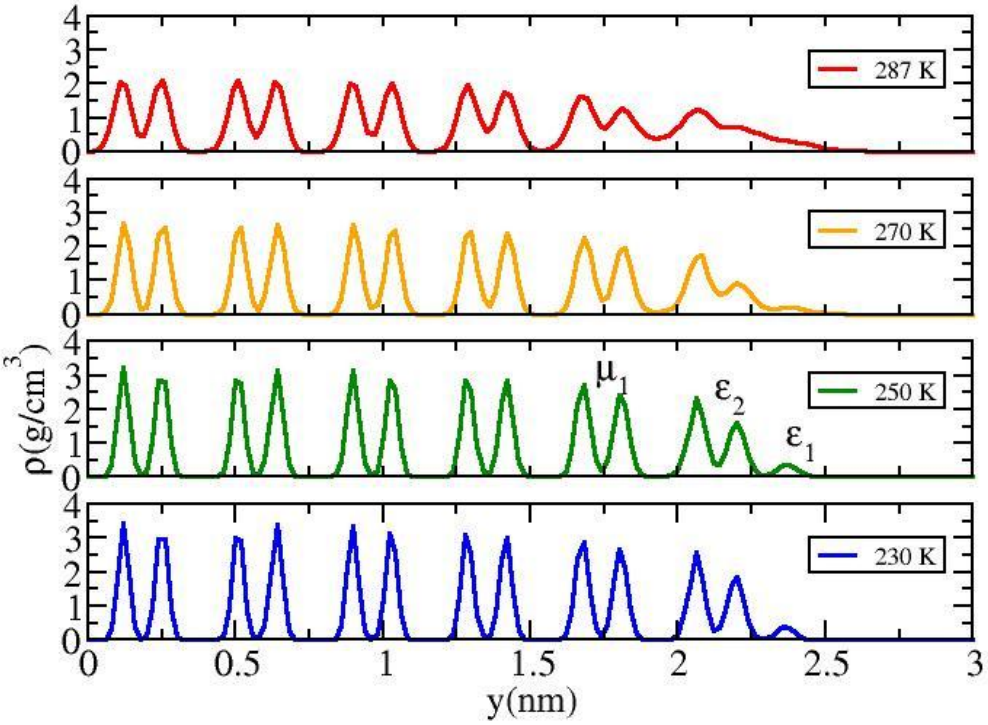

Figure 4.

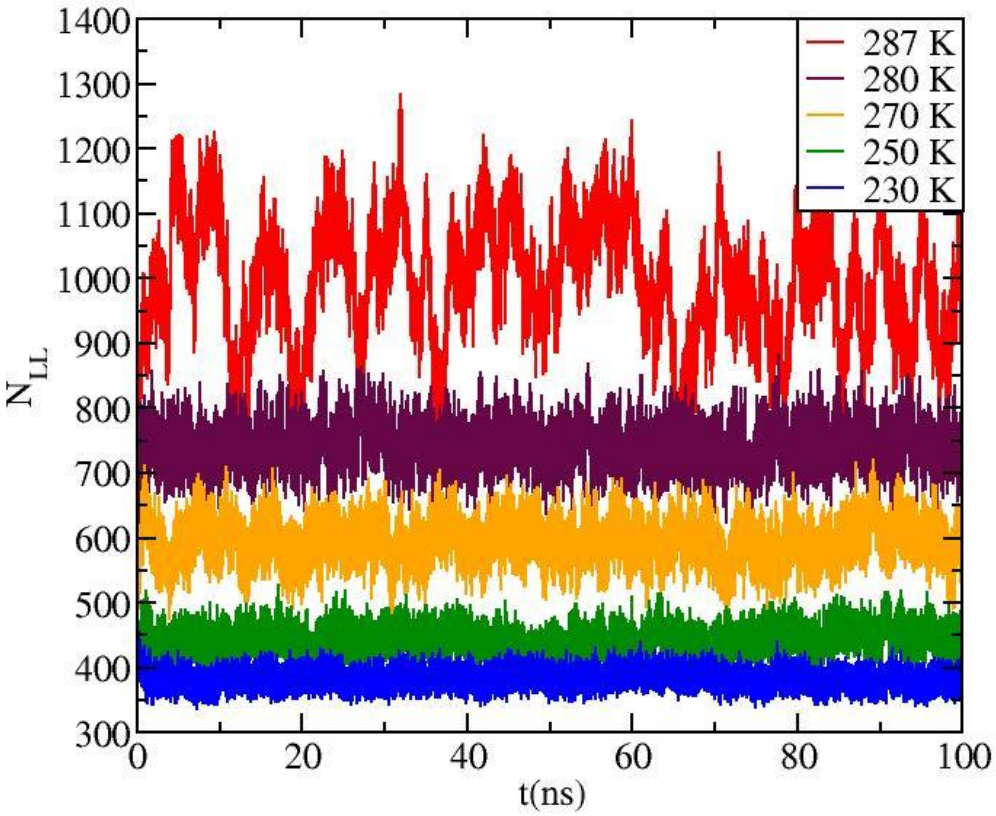
1400
1300
1200
1100
1000
900
800
700
600
500
400
300
N_LL
0
20
40
60
80
100
t(ns)
287 K
280 K
270 K
250 K
230 K

Figure 5.

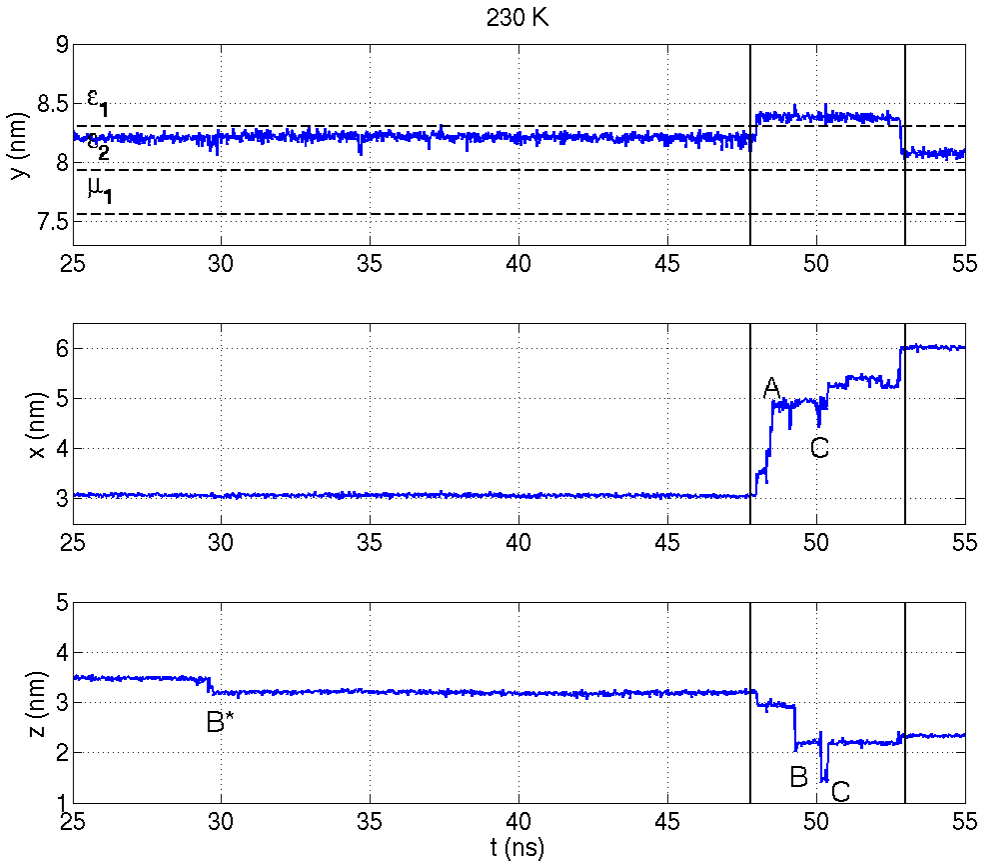

Figure 6.

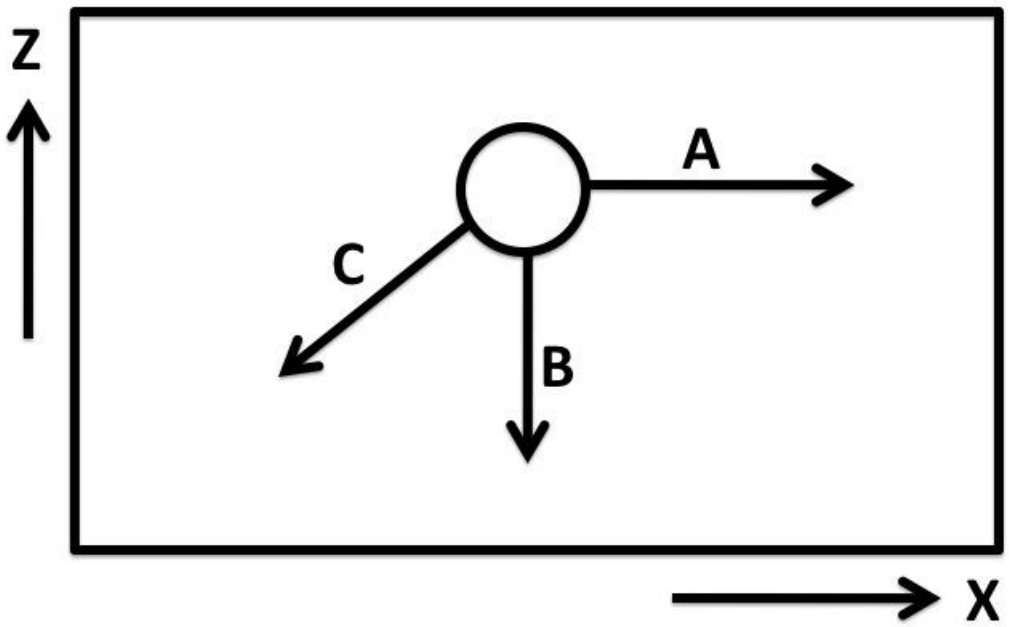

Figure 7.

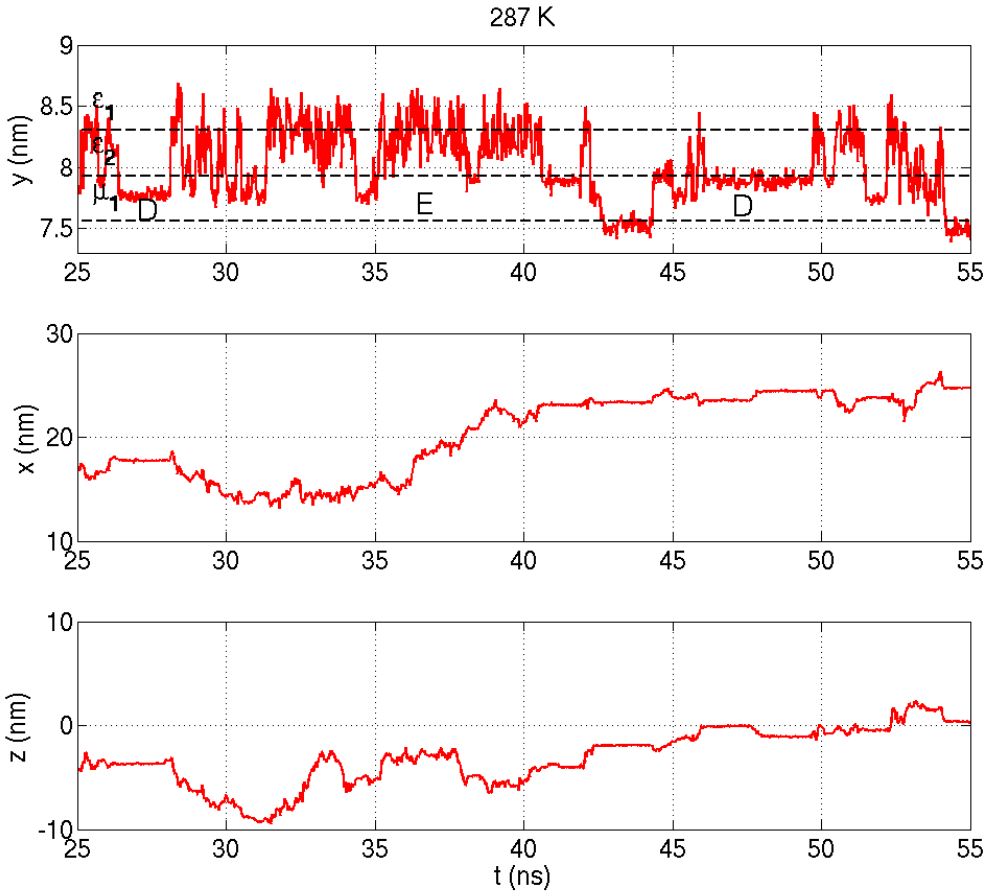

Figure 8.

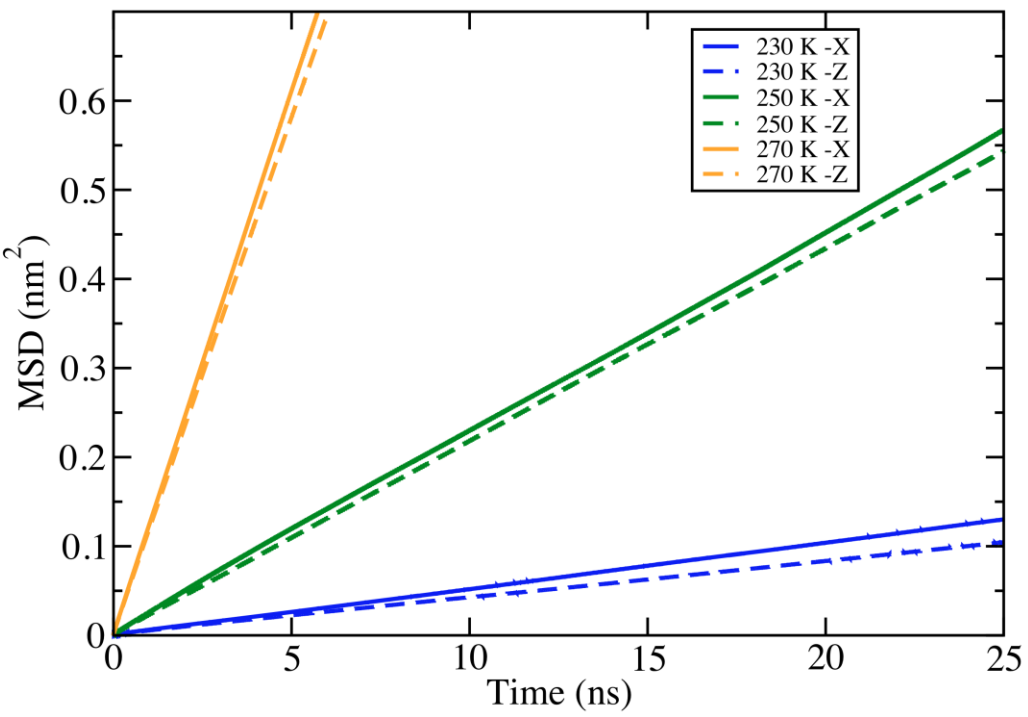
230 K -X
230 K -Z
250 K -X
250 K -Z
270 K -X
270 K -Z
MSD (nm^2)
0
0.1
0.2
0.3
0.4
0.5
0.6
0
5
10
15
20
25
Time (ns)

Figure 9.

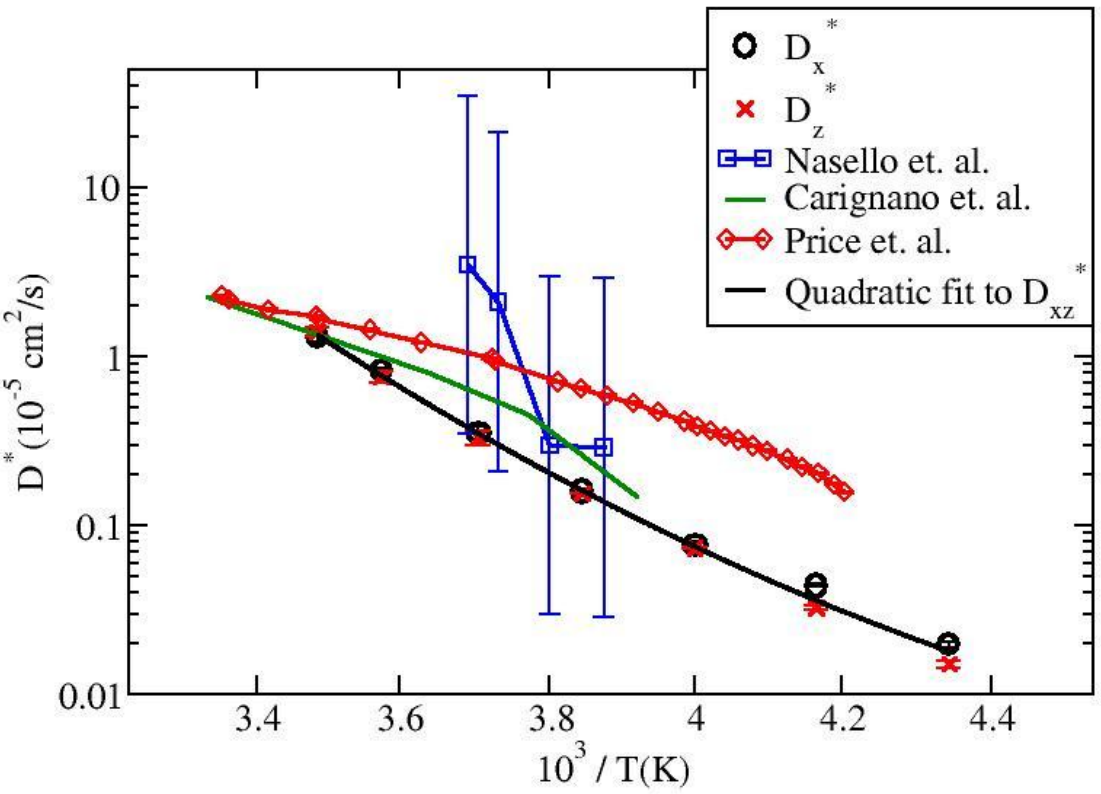
D*x
D*z
Nasello et. al.
Carignano et. al.
Price et. al.
Quadratic fit to D*xz
10
1
0.1
0.01
D* (10-5 cm2/s)
3.4
3.6
3.8
4
4.2
4.4
10^3 / T(K)

Figure 10.

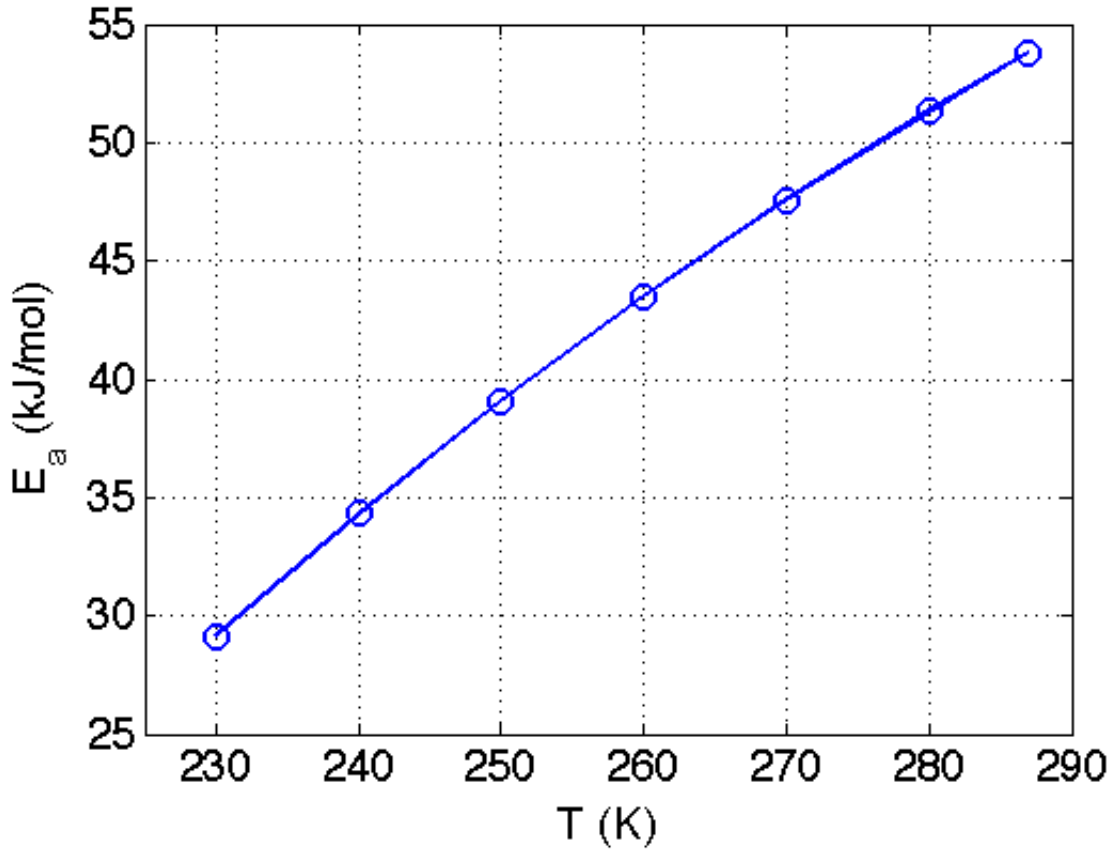

Figure 11.

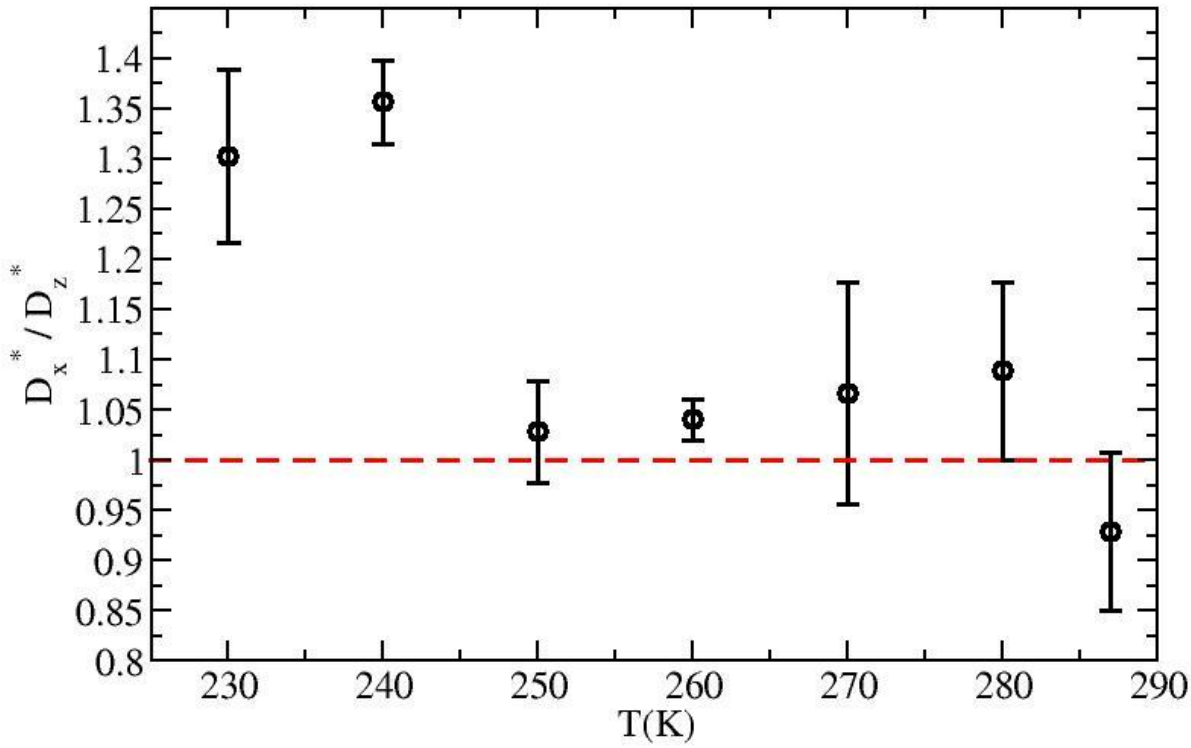
1.4
1.35
1.3
1.25
1.2
1.15
1.1
1.05
1
0.95
0.9
0.85
0.8
D_x^* / D_z^*
230
240
250
260
270
280
290
T(K)